applied optics

Enhanced two-frequency phase-shifting method

JAE-SANG HYUN AND SONG ZHANG*

School of Mechanical Engineering, Purdue University, West Lafayette, Indiana 47907, USA
**Corresponding author: szhang15@purdue.edu*

Received 17 March 2016; accepted 5 May 2016; posted 6 May 2016 (Doc. ID 261417); published 27 May 2016

One of the major challenges of employing a two-frequency (or two-wavelength) phase-shifting algorithm for absolute three-dimensional shape measurement is its sensitivity to noise. Therefore, three- or more-frequency phase-shifting algorithms are often used in lieu of a two-frequency phase-shifting algorithm for applications where the noise is severe. This paper proposes a method to use geometric constraints of digital fringe projection system to substantially reduce the noise impact by allowing the use of more than one period of equivalent phase map for temporal phase unwrapping. Experiments successfully verified the enhanced performance of the proposed method without increasing the number of patterns.

OCIS codes: (120.0120) Instrumentation, measurement, and metrology; (120.2650) Fringe analysis; (100.5070) Phase retrieval.

http://dx.doi.org/10.1364/AO.55.004395

1. INTRODUCTION

High-speed and high-accuracy three-dimensional (3D) shape measurement is of great interest to numerous applications, including *in situ* quality control in manufacturing and disease diagnosis in medical practices.

Among all 3D shape measurement techniques developed, phase-based methods using fringe analysis techniques uniquely stand out due to their measurement speeds and accuracy. Retrieving phase from a sequence of phase-shifted fringe patterns is one of most popular methods since they can recover phase for each point, are less sensitive to surface reflectivity variations, etc. Typically, the phase directly obtained from fringe patterns can only provide phase value ranging from $-\pi$ to $+\pi$, and a phase-unwrapping algorithm has to be adopted to recover a continuous phase map. Phase unwrapping can be classified into spatial and temporal phase unwrapping categories. The spatial phase unwrapping determines 2π discontinuous locations from the phase map itself and adds or subtracts multiple number of 2π accordingly. Numerous phase-unwrapping algorithms have been developed with some being fast but less robust and some being robust but slow; the principles and various spatial phase-unwrapping algorithms have been summarized in [1]. Among those spatial phase-unwrapping algorithms, the popular ones are reliability-guided phase-unwrapping algorithms since they tend to be robust. Different reliability-guided phase-unwrapping algorithms have been reviewed in [2]. Regardless the robustness of any spatial phase-unwrapping algorithms, they typically only generate a *relative* phase map that is relative to a point for each connected component. Therefore, 3D reconstructed shape using a spatial phase-unwrapping algorithm usually only provides relative geometry to that point instead of absolute geometry. Furthermore, most spatial phase-unwrapping algorithms fail if abrupt surface changes introduce more than 2π phase changes from one point to the next point.

Temporal phase unwrapping, in contrast, tries to fundamentally eliminate the problem of spatial phase unwrapping by capturing more images. And one of the popular methods is to use multifrequency (or wavelength) phase-shifting techniques [3–5], where fringe patterns with different fringe periods are used to generate equivalent phase map, ϕ^{eq}. If the equivalent phase map ranging from $-\pi$ to π covers the whole range of the surface, no phase unwrapping is necessary and thus ϕ^{eq} can be regarded as the unwrapped phase, or $\Phi^{eq} = \phi^{eq}$. Φ^{eq} can then be used to determine the fringe order for each point on the high-frequency phase for temporal phase unwrapping.

Multifrequency phase-unwrapping algorithms were developed for laser interferometry systems. Due to the flexibility of digital fringe projection (DFP) techniques, more temporal phase-unwrapping algorithms have been developed, including gray-coding plus phase-shifting methods [6,7], spatial coding plus phase-shifting methods [8], and phase-coding plus phase-shifting methods [9–11]. Compared to the two-frequency phase-shifting based temporal phase-unwrapping method, the gray-coding methods typically require more than three additional binary patterns to determine fringe orders. The method of spatial coding requires the knowledge of neighborhood pixel information, and could fail if the surface is not locally smooth. Phase-coding methods only need three additional fringe patterns, yet it is difficult to differentiate the encoded fringe orders if the noise is large, which is the same problem as conventional two-frequency phase-shifting methods.

It is desirable for high-speed applications to use fewer fringe patterns to reconstruct one 3D frame, and thus the two-frequency phase-shifting algorithm is preferable. Yet, large noise could completely fail the fringe order determination, as thoroughly discussed by Creath [12]. Conventionally, multi-frequency phase-shifting algorithms are often used in lieu of the two-frequency phase-shifting algorithm for applications where noise is severe. This paper proposes a method to enhance the robustness of the two-frequency phase-shifting method yet not to increase the number of patterns captured. In lieu of using more patterns, this proposed method uses geometric constraints of the DFP system to reduce the noise impact by allowing the use of more than one period of equivalent phase map to determine fringe order. Experiments demonstrated that noise impact on phase unwrapping can be reduced by a factor of 4 or even higher.

Section 2 explains the principles of the proposed method to enhance the two-frequency phase-shifting algorithm by using minimum phase. Section 3 shows some simulation results to validate the proposed method. Section 4 presents experimental results to further validate the proposed method. Lastly, Section 5 summarizes the paper.

2. PRINCIPLE

This section thoroughly explains the principle of the proposed two-frequency phase-shifting method. Specifically, we will present the basics of the two-frequency phase-shifting algorithm, detail the minimum phase generation using geometric constraints of the calibrated DFP system, and explain how to use the minimum phase to enhance the two-frequency phase-shifting method.

A. Two-Frequency Phase-Shifting Algorithm

As aforementioned, phase-shifting algorithms are extensively used in optical metrology. Over the years, numerous phase-shifting algorithms have been developed including three-step, four-step, and least-squares [13]. For high-speed applications, a three-step phase-shifting algorithm is desirable since it uses the minimum number of patterns to recover phase. For a three-step phase-shifting algorithm with equal phase shifts, three fringe images can be mathematically described as

$$I_1(x,y) = I'(x,y) + I''(x,y)\cos(\phi - 2\pi/3), \tag{1}$$

$$I_2(x,y) = I'(x,y) + I''(x,y)\cos(\phi), \tag{2}$$

$$I_3(x,y) = I'(x,y) + I''(x,y)\cos(\phi + 2\pi/3), \tag{3}$$

where $I'(x,y)$ is the average intensity, $I''(x,y)$ is intensity modulation, and ϕ is the phase to be solved for. Solving Eqs. (1)–(3) simultaneously leads to

$$\phi(x,y) = \tan^{-1}\left[\frac{\sqrt{3}(I_1 - I_3)}{2I_2 - I_1 - I_3}\right]. \tag{4}$$

The phase obtained from Eq. (4) ranges from $-\pi$ to π with 2π discontinuities, and this phase is called the wrapped phase. The process of removing 2π discontinuities to obtain a continuous phase map is called phase unwrapping. As discussed in Section 1, there are two types of phase-unwrapping methods: spatial and temporal, with spatial algorithms being limited to smooth and continuous phase reconstruction and temporal algorithms being more general but requiring additional information.

One of the temporal phase-unwrapping methods is to use multifrequency phase-shifted fringe patterns, where fringe patterns with different fringe periods are used to generate an equivalent phase map, ϕ^{eq}. If the equivalent phase map ranges from $-\pi$ to π for the whole surface, no phase unwrapping is necessary. Therefore, ϕ^{eq} can be regarded as unwrapped phase $\Phi^{eq} = \phi^{eq}$. Φ^{eq} can be used to determine fringe order for each point on the high-frequency phase for temporal phase unwrapping. For high-speed measurement, a two-frequency phase-shifting algorithm is preferable comparing to three- or more-frequency phase-shifting algorithms since it uses fewer images for 3D reconstruction.

From two-frequency phase-shifted fringe patterns, one can obtain two wrapped phase maps $\phi^1(x,y)$ and $\phi^2(x,y)$. The equivalent phase map can be computed as

$$\phi^{eq}(x,y) = \phi^1(x,y) - \phi^2(x,y) \bmod 2\pi, \tag{5}$$

where mod is the modulus operation. If the equivalent phase, ϕ^{eq}, does not have any 2π discontinuities, it can be regarded as unwrapped phase Φ^{eq} and be used to unwrap $\phi^1(x,y)$ and $\phi^2(x,y)$ pixel by pixel.

For a DFP system, the frequency of a fringe pattern is actually defined as $1/T$, where T is fringe period in pixel. If the fringe periods used for a two-frequency phase-shifting algorithm are T^1 and T^2, it is straightforward to prove that the equivalent fringe period to generate the equivalent phase is

$$T^{eq} = \frac{T^1 T^2}{T^2 - T^1}, \tag{6}$$

assuming $T^2 > T^1$.

Therefore, the condition to use a two-frequency phase-shifting algorithm for temporal phase unwrapping is that T^{eq} is the whole projection range. In such a case, the fringe order for high-frequency $1/T^1$ can be determined by

$$K(x,y) = \text{Round}\left[\frac{\phi^{eq}(x,y)\frac{T^{eq}}{T^1} - \phi^1(x,y)}{2\pi}\right], \tag{7}$$

to temporally unwrap $\phi^1(x,y)$ by

$$\Phi^1(x,y) = \phi^1(x,y) + K(x,y) \times 2\pi. \tag{8}$$

Here Round() is to round a floating point number to its closest integer number, and $\Phi^1(x,y)$ is the unwrapped phase of $\phi^1(x,y)$.

The two-frequency phase-unwrapping algorithm discussed above works in principle, yet has two major limitations:

1. *Limited frequency choice*. It is well known that using higher-frequency (or smaller T) fringe patterns can generate accurate phase, and thus it is preferable to use smaller T for higher accuracy 3D shape measurement. However, the two-frequency phase-shifting algorithm limits its choices. For example, if a three-step phase-shifting algorithm is used, it is preferable to use a fringe period of $n \times 3$ pixels (here n is an integer) to avoid phase shift error. Based on this constraint, in order to generate $T^{eq} = 1024$ pixels, the smallest fringe periods to use are

$T^1 = 54$ pixels and $T^2 = 57$ pixels, which are very large compared to the desired value of around 30 pixels.

2. *Large noise impact*. From Eq. (7), one may notice that the equivalent phase ϕ^{eq} is scaled up by a scaling factor of T^{eq}/T^1 to determine fringe order $K(x, y)$. It is important to note that the noise in ϕ^{eq} is also proportionally scaled up by a factor of T^{eq}/T^1. This scaled noise could lead to incorrectly determine fringe order, $K(x, y)$. For example, if the phase noise is 0.2 rad, a scaling factor of 18 could lead to incorrect fringe orders.

Due to the flexibility of digital fringe pattern generation, the DFP methods mitigate the former limitation by directly projecting the equivalent frequency fringe patterns such that one single fringe covers the whole projection range (e.g., $T^2 = T^{eq} = 1024$ pixels for a projector resolution of 1024×768) and then use $\phi^2(x, y) = \phi^{eq}(x, y)$ to unwrap ϕ^1. By doing so, it allows the use of higher-frequency fringe patterns (e.g., $T^1 = 30$ pixels). The consequence of using such an approach is that the noise problem could be amplified since the scaling factor T^{eq}/T^1 could be even larger. For example, if $T^2 = 1024$ and $T^1 = 30$ pixels, the scaling factor is 34; and the phase noise larger than 0.1 rad for a point can lead to a wrong fringe order. As a result, the two-frequency phase-shifting method is not very appealing to practical applications, and three- or more frequency phase-shifting algorithms are more extensively used.

One may realize that the fundamental problem associated with the aforementioned two-frequency phase-shifting algorithm is its requirement that T^{eq} is large enough to cover the whole measurement range. If this strong requirement is relaxed, the two-frequency phase-shifting algorithms could be substantially enhanced.

In this research, we propose to use the geometric constraints of DFP systems to improve the performance of two-frequency phase-shifting algorithms. To understand such an approach, we will introduce the mathematical model of a DFP system and how to use such a model to set up constraints for temporal phase unwrapping such as smaller T^{eq} can be used.

B. DFP System Model

In this research, we use a well-known pinhole model to describe an imaging lens. This model essentially describes the relationship between 3D world coordinates (x^w, y^w, z^w) and its projection onto 2D imaging coordinates (u, v). The linear pinhole model can be mathematically described as

$$s\begin{bmatrix} u \\ v \\ 1 \end{bmatrix} = \mathbf{A}[\mathbf{R} \quad \mathbf{t}]\begin{bmatrix} x^w \\ y^w \\ z^w \\ 1 \end{bmatrix}, \tag{9}$$

where

$$\mathbf{R} = \begin{bmatrix} r_{11} & r_{12} & r_{13} \\ r_{21} & r_{22} & r_{23} \\ r_{31} & r_{32} & r_{33} \end{bmatrix}, \tag{10}$$

$$\mathbf{t} = \begin{bmatrix} t_1 \\ t_2 \\ t_3 \end{bmatrix}, \tag{11}$$

$$\mathbf{A} = \begin{bmatrix} f_u & \gamma & u_0 \\ 0 & f_v & v_0 \\ 0 & 0 & 1 \end{bmatrix}, \tag{12}$$

respectively, represent the rotation $\mathbf{R}$ and the translation $\mathbf{t}$ from the world coordinate system to the lens coordinate system, and the projection $\mathbf{A}$ from the lens coordinate system to the 2D image coordinate system. s is a scaling factor; f_u and f_v are the effective focal lengths; γ is the skew factor of u and v axes, and for research-grade cameras $\gamma = 0$; and (u_0, v_0) is the principle point, the intersection of the optical axis with the imaging plane.

For simplicity, let us define the projection matrix $\mathbf{P}$ as

$$\mathbf{P} = \mathbf{A}[\mathbf{R} \quad \mathbf{t}] = \begin{bmatrix} p_{11} & p_{12} & p_{13} & p_{14} \\ p_{21} & p_{22} & p_{23} & p_{24} \\ p_{31} & p_{32} & p_{33} & p_{34} \end{bmatrix}, \tag{13}$$

which can be estimated from calibration.

The same lens model is applicable to both the projector and the camera, and the only difference is that the projector is the inverse of a camera. Therefore, if the camera and the projector are calibrated under the same world coordinate system, we have

$$s^p[u^p \quad v^p \quad 1]^t = \mathbf{P^p}[x^w \quad y^w \quad z^w \quad 1]^t, \tag{14}$$

$$s^c[u^c \quad v^c \quad 1]^t = \mathbf{P^c}[x^w \quad y^w \quad z^w \quad 1]^t. \tag{15}$$

Here superscript p represents the projector, superscript c presents the camera, and superscript t represents the transpose of a matrix. After calibration, $\mathbf{P^p}$ and $\mathbf{P^c}$ are known.

C. Temporal Unwrapping Use Minimum/Maximum Phase Maps

For any given calibrated DFP system, the calibration volume is well known, which defines minimum z, z_{min}, and maximum z, z_{max}. Practically, z_{min} and z_{max} can be defined as the interested region of z range within the calibration volume.

From Eq. (15), if z^w is known, for any given pixel (u^c, v^c), coordinates x^w and y^w can be uniquely solved. Once (x^w, y^w, z^w) coordinates of a given point (u^c, v^c) are known, its corresponding point on the projector (u^p, v^p) can be computed using Eq. (14). Because the phase on the projector is well defined for any given pixel (even multiple fringe periods), the camera phase map can be built for a given z^w value, and such a phase map does not have any 2π ambiguities. Therefore we can create two phase maps Φ_{min} and Φ_{max} that respectively correspond to z_{min} and z_{max}.

Figure 1 illustrates the basic concepts of using minimum phase, Φ_{min}, to correct 2π discontinuities. Assume the region on the projector that a camera captures at $z = z_{min}$ is shown in the red dashed window, the phase directly obtained from three-phase-shifted fringe patterns has one 2π jump, ϕ_1, as shown in Fig. 1(a). However, since such a phase is well defined on the projector, the Φ_{min} can be obtained, which is a continuous phase on the projector space, as shown in Fig. 1(b). The cross sections of the phase maps are shown in Fig. 1(c). This example shows that if the wrapped phase is below Φ_{min}, 2π should be added to the phase to unwrap it. One may also notice that even if the phase is obtained at z_{max}, the condition of adding 2π to ϕ_2 is still the same: when $\phi_2 < \Phi_{min}$.

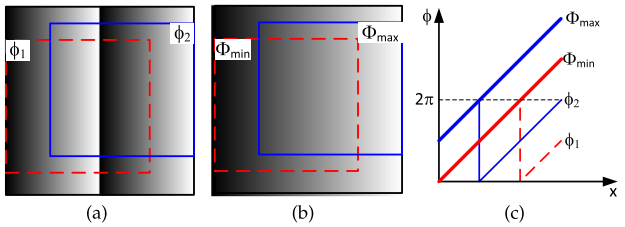

Fig. 1. Conceptual idea of removing 2π jumps of low-frequency phase map by using the minimum phase map determined from geometric constraints. (a) Windowed regions show phase maps acquired by the camera at different depths z: red dashed window shows at z_{min} and solid blue window shows at z_{max}; (b) corresponding Φ_{min} and Φ_{max} defined on the projector; (c) cross sections of Φ_{min} and Φ_{max} and the wrapped phase maps with 2π discontinuities.

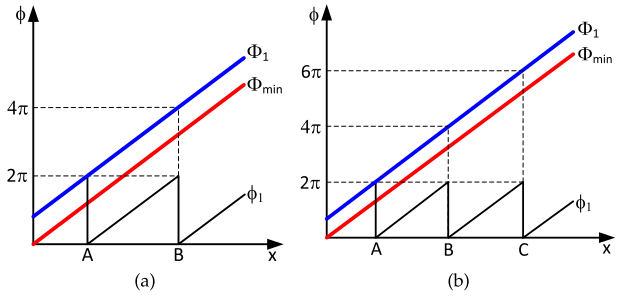

Fig. 2. Determination of number of 2π to be added by using Φ_{min} when low-frequency phase has multiple 2π jumps. (a) Example of having two 2π jumps; (b) example of having three 2π jumps.

The above example demonstrates that the equivalent phase ϕ^{eq} does not have to be continuous across the whole area: it is fine to have one 2π jump. This indicates that the scaling factor T^{eq}/T^1 can be half of the required value, leading to reducing the noise impact by a factor of 2.

The question is: can we increase the number of 2π jumps and still properly find them using the geometric constraints (or Φ_{min}) to remove them? Figure 2 illustrates the cases for two and three jumps. Figure 2(a) shows a case where there are two 2π jump locations, A and B. Between A and B, the phase difference $\Phi_{min} - \phi_1$ is larger than 0 but less than 2π; but on the right of Point B, the phase difference is larger than 2π. Therefore, 2π should be added to unwrap the point between A and B, and 4π should be added on the right side of Point B.

For cases with three jumps shown in Fig. 2(b), if $0 < \Phi_{min} - \phi_1 < 2\pi$, 2π (i.e., between A and B) should be added; $2\pi < \Phi_{min} - \phi_1 < 4\pi$ (i.e., between B and C), 4π should be added; and $4\pi < \Phi_{min} - \phi_1 < 6\pi$ (i.e., beyond C), 6π should be added. A similar approach can be used to determine the number of 2π to be added for the equivalent phase.

As aforementioned, the use of 2π jumps for the equivalent phase for temporal phase unwrapping is to reduce the scaling factor. If N number of jumps are used, the scaling factor T^{eq}/T^1 can be reduced by a factor of $N+1$, and thus reduce the noise impact to $1/(N+1)$ times.

3. SIMULATIONS

Simulations were performed to demonstrate the viability of the proposed method to improve the two-frequency phase-shifting algorithm. Figure 3 shows an example that fails standard two-frequency phase unwrapping when the high-frequency phase has a fringe period of $T^1 = 30$ pixels and the low-frequency phase has a fringe period of $T^2 = 1024$ pixels. In this simulation, Gaussian noise was added such that the signal-to-noise ratio (SNR) is 25. Figure 3(a) shows three phase-shifted high-frequency fringe patterns, and Fig. 3(b) shows a close-up view of the fringe patterns. As can be seen, the fringe patterns are noisy. Figure 3(c) shows the phase can be computed using Eq. (4), and its zoom-in view is shown in Fig. 3(d). The low-frequency fringe patterns and the phase are respectively shown in Figs. 3(e) and 3(f). Directly applying

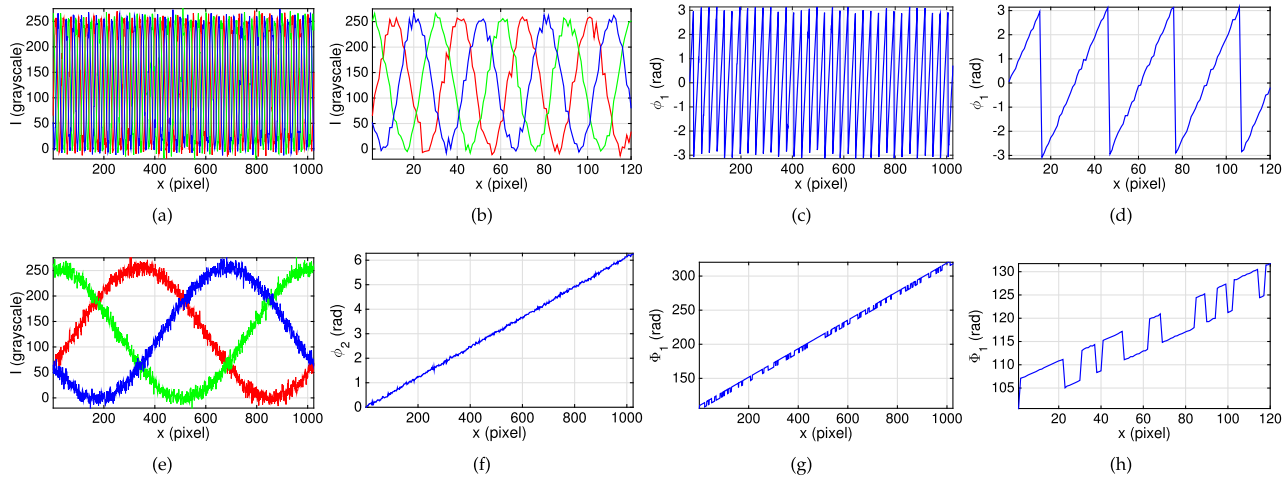

Fig. 3. Simulation result of standard two-frequency phase unwrapping when the SNR is not high (for this example, SNR = 25). (a) Three high-frequency phase-shifted fringe patterns with phase shifts of $2\pi/3$ and fringe period of $T = 30$ pixels; (b) zoom-in view of fringe patterns shown in (a); (c) wrapped phase of the high-frequency fringe patterns; (d) zoom-in view of the high-frequency phase; (e) low-frequency fringe patterns; (f) low-frequency phase; (g) unwrapped high-frequency phase; (h) zoom-in-view of the unwrapped high-frequency phase.

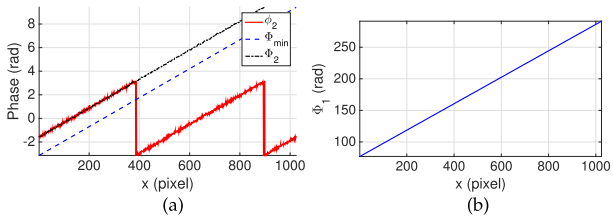

Fig. 4. Example of using one jump on the low-frequency phase and geometric constraints to unwrap the high-frequency phase. (a) Original low frequency phase ϕ_2, the phase at $z_{\min}$ from geometric constraints $\Phi_{\min}$, and the unwrapped low-frequency phase Φ_2; (b) unwrapped high-frequency phase Φ_1.

the conventional two-frequency phase unwrapping will generate the phase map shown in Fig. 3(g). Clearly, the phase is not smooth with many points being incorrectly unwrapped. Figure 3(h) shows a closed-up view of the unwrapped phase, showing that the incorrectly unwrapped phase points cannot be filtered out by filters since there are many successive points.

We then added one jump to the low-frequency fringe patterns and use the geometric constraints to remove 2π jumps of the low-frequency phase, as shown in Fig. 4(a). By using the unwrapped phase with one jump, the high-frequency phase shown in Fig. 3(c) can be properly unwrapped, as shown in Fig. 4(b).

4. EXPERIMENT

To verify the performance of the proposed method, we developed a DFP system that includes a complementary metal-oxide semiconductor camera (Model: Vision Research Phantom V9.1), a digital light processing projector (Model: Texas Instruments LightCrafter 4500), and a microprocessor (Model: Arduino Uno). The camera is attached with a 24 mm focal length lens (Model: SIGMA 24 mm f/1.8 EX DG). The camera resolution selected was 1024 × 1024, and the image data was transferred to a computer via an ethernet cable. The resolution of the projector is 912 × 1140. The microprocessor was used to synchronize the camera with the projector. The system was calibrated using the method discussed in [14]. For all experiments presented in this paper, horizontal fringe patterns are generated by computer and projected by the projector. Since the projector's vertical resolution is 1140 pixels, the equivalent fringe period has to be $T^{\text{eq}} = 1140$ pixels in order to temporally unwrap high-frequency phase if a conventional two-frequency phase-shifting algorithm is used.

We experimentally verified the performance of the enhanced two-frequency phase-shifting method. We first test the case when fringe patterns are of high quality (i.e., high SNR). Figure 5(a) shows the photograph of the statue we measured. It is important to note that we did not show the full resolution image of 1024 × 1024 because the rest areas are simply the background; and we crop the image the same way for all images for clearer visualization. In this experiment, the high-frequency fringe patterns use fringe periods of $T^1 = 30$ pixels. One of the high-frequency fringe patterns and the wrapped phase map are, respectively, shown in Figs. 5(b) and 5(c). If a conventional two-frequency phase-shifting algorithm is

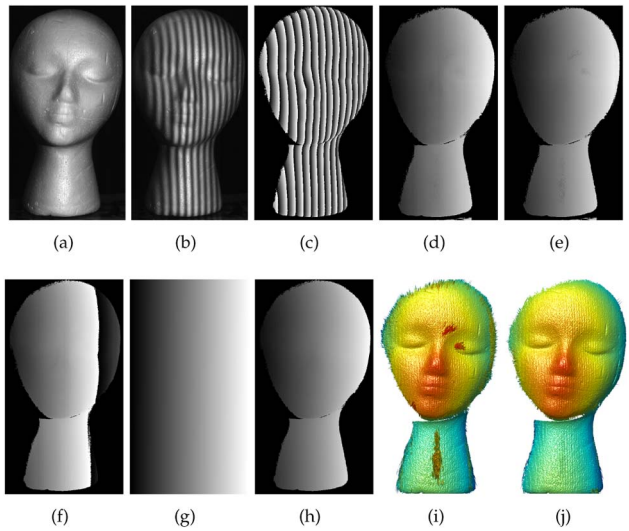

Fig. 5. Comparison of the conventional two-frequency phase-shifting algorithm and the proposed enhanced algorithm when the fringe patterns are of high quality. (a) Photograph of the measured statue; (b) one of the captured high-frequency fringe patterns; (c) wrapped phase from high-frequency fringe patterns; (d) wrapped phase from low-frequency fringe patterns with fringe period of 1140 pixels; (e) unwrapped phase using the conventional two-frequency phase-shifting algorithm; (f) wrapped phase from low-frequency fringe patterns with fringe period of 380 pixels; (g) minimum wrapped phase $\Phi_{\min}$; (h) unwrapped phase using the proposed method; (i) 3D result using the conventional two-frequency phase-shifting method; (j) 3D result using the proposed two-frequency phase-shifting method.

applied, the low-frequency fringe patterns have a fringe period of $T^2 = 1140$ pixels, and the corresponding wrapped phase is shown in Fig. 5(d). Applying a conventional two-frequency phase-shifting algorithm results in the unwrapped phase shown in Fig. 5(e). As one might see, the unwrapped phase

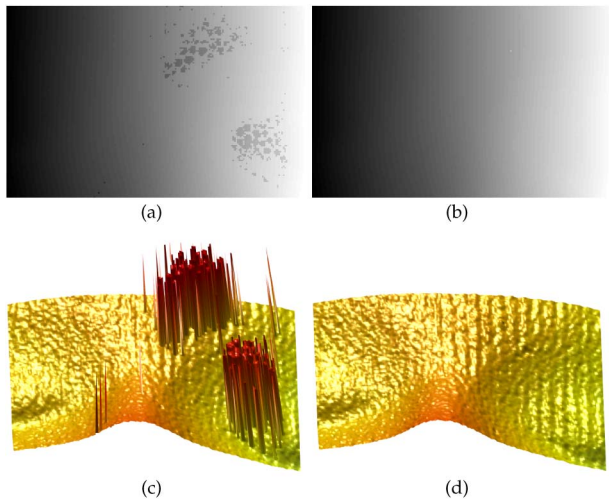

Fig. 6. Close-up views of the results from Fig. 5 around the eye region. (a) Zoom-in view of the unwrapped phase map shown in Fig. 5(e); (b) zoom-in view of the unwrapped phase map shown in Fig. 5(h); (c) zoom-in view of 3D result shown in Fig. 5(i); (d) zoom-in view of 3D result shown in Fig. 5(j).

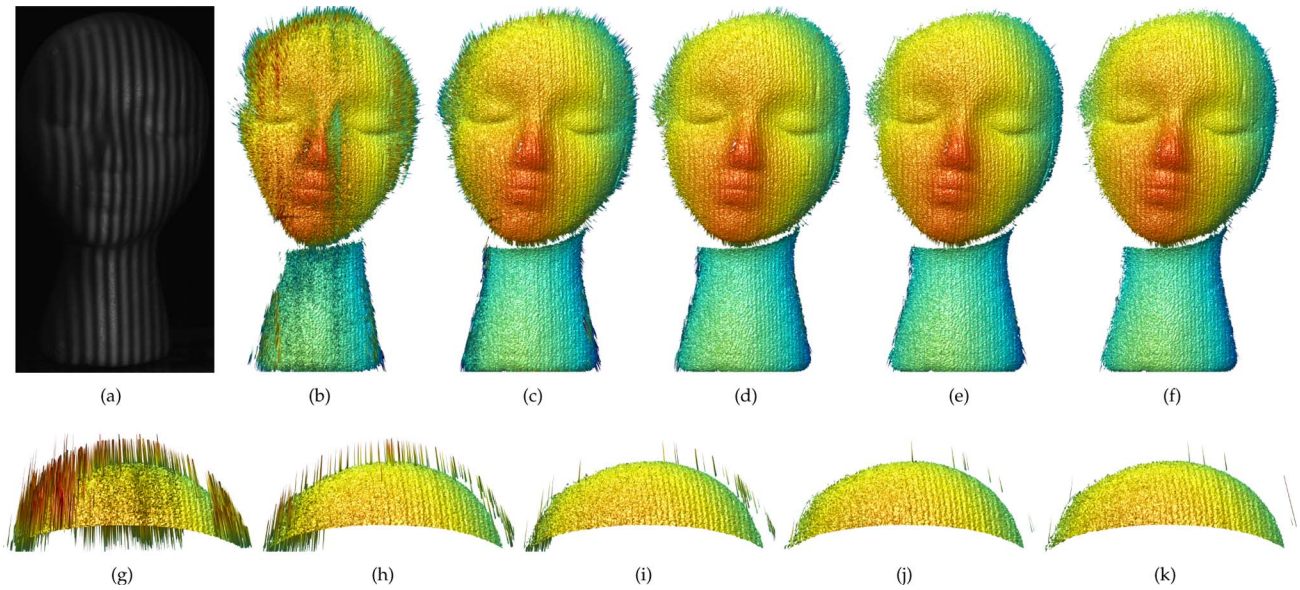

Fig. 7. Comparison of the conventional two-frequency phase-shifting algorithm and the proposed enhanced algorithm when the fringe patterns have low SNR. (a) One of the captured high-frequency fringe patterns; (b) 3D result using the conventional two-frequency phase-shifting method; (c)–(f) 3D results using the proposed two-frequency phase-shifting method when low-frequency fringe patterns use two (c), three (d), four (e), and five (f) periods of sinusoidal fringes, respectively; (g)–(k) zoom-in views of the same regions for results shown in (b)–(f).

is not smooth on the neck and around the right eye regions, indicating some areas of the phase are not correctly unwrapped.

In contrast, if the proposed method is used, the low-frequency fringe pattern can have multiple fringes. For example, we can use a fringe period of $T^2 = 380$ pixels to reduce the noise impact. Figure 5(f) shows the wrapped phase map. The minimum phase map determined from geometric constraints of the corresponding region is shown in Fig. 5(g). Figure 5(h) shows the unwrapped phase map using the proposed method. This phase map is smooth overall. Once the unwrapped phase map is obtained, 3D shape can be reconstructed. Figures 5(i) and 5(j) respectively show 3D reconstruction using the conventional two-frequency phase-shifting algorithm and that using our proposed algorithm.

To better visualize differences, Fig. 6 shows the closed-up view of the unwrapped phase maps and the corresponding 3D reconstructions. The 3D result from our proposed method does not have spiky noisy points that are apparent on the result from the conventional algorithm. These experiments clearly demonstrated that even for high-quality fringe patterns, the conventional two-frequency phase-shifting algorithm could still fail to correctly unwrap the phase due to the large scaling factor T^{eq}/T^1. In comparison, the proposed method does not have such a problem.

To further verify the performance of the proposed method, we measured the same statue with low fringe quality to emulate low SNR cases. Figure 7(a) shows one of the capture high-frequency fringe patterns; clearly the pattern has low SNR. Figure 7(b) shows 3D results from the conventional two-frequency phase-shifting algorithm. The whole surface is poorly measured with spiky points present everywhere, as anticipated. In contrast, if we use the proposed method to perform measurement under exactly the same settings, the 3D results are shown in Figs. 7(c)–7(f) with different numbers of jumps ranging from 1 to 4. To better visualize the differences, we showed zoom-in views of the overhead area for all these results, as shown in Figs. 7(g)–7(k). They all greatly reduced incorrectly unwrapped points with more jumps providing better results. However, one may notice that, for such a low SNR case, using one jump (or two periods for low-frequency fringe patterns) is not sufficient, but using five periods of fringe patterns can almost eliminate all incorrectly unwrapped points. It should be noted that by using five periods of fringe patterns, the proposed method reduces the noise impact by a factor of 5. These experiments further demonstrated that the proposed two-frequency phase-shifting algorithm can indeed greatly enhance the performance of the conventional two-frequency phase-shifting algorithm by using the minimum phase.

5. SUMMARY

This paper has presented a method to substantially improve the conventional two-frequency phase-shifting algorithm by using geometric constraints of the DFP system. We demonstrated that the noise impact can be substantially reduced by allowing the use of more than one period of equivalent phase map to determine fringe order. Both simulation and experiments successfully verified the drastic improvements of the proposed method over the conventional two-frequency phase-shifting algorithm. Since the proposed method does not require more fringe patterns to be captured, it has the advantage of measurement speeds for high-speed applications.

Funding. Directorate for Engineering (ENG) (100000084, CMMI-1521048).

Acknowledgment. The views expressed in this paper are those of the authors and not necessarily those of the NSF.

REFERENCES

1. D. C. Ghiglia and M. D. Pritt, eds., *Two-Dimensional Phase Unwrapping: Theory, Algorithms, and Software* (Wiley, 1998).
2. X. Su and W. Chen, "Reliability-guided phase unwrapping algorithm: a review," Opt. Laser Eng. **42**, 245–261 (2004).
3. Y.-Y. Cheng and J. C. Wyant, "Two-wavelength phase shifting interferometry," Appl. Opt. **23**, 4539–4543 (1984).
4. Y.-Y. Cheng and J. C. Wyant, "Multiple-wavelength phase shifting interferometry," Appl. Opt. **24**, 804–807 (1985).
5. D. P. Towers, J. D. C. Jones, and C. E. Towers, "Optimum frequency selection in multi-frequency interferometry," Opt. Lett. **28**, 887–889 (2003).
6. G. Sansoni, M. Carocci, and R. Rodella, "Three-dimensional vision based on a combination of gray-code and phase-shift light projection: analysis and compensation of the systematic errors," Appl. Opt. **38**, 6565–6573 (1999).
7. Q. Zhang, X. Su, L. Xiang, and X. Sun, "3-d shape measurement based on complementary gray-code light," Opt. Laser Eng. **50**, 574–579 (2012).
8. Y. Li, H. Jin, and H. Wang, "Three-dimensional shape measurement using binary spatio-temporal encoded illumination," J. Opt. A **11**, 075502 (2009).
9. Y. Wang and S. Zhang, "Novel phase coding method for absolute phase retrieval," Opt. Lett. **37**, 2067–2069 (2012).
10. C. Zhou, T. Liu, S. Si, J. Xu, Y. Liu, and Z. Lei, "Phase coding method for absolute phase retrieval with a large number of codewords," Opt. Express **20**, 24139–24150 (2012).
11. C. Zhou, T. Liu, S. Si, J. Xu, Y. Liu, and Z. Lei, "An improved stair phase encoding method for absolute phase retrieval," Opt. Laser Eng. **66**, 269–278 (2015).
12. K. Creath, "Step height measurement using two-wavelength phase-shifting interferometry," Appl. Opt. **26**, 2810–2816 (1987).
13. D. Malacara, ed., *Optical Shop Testing*, 3rd ed. (Wiley, 2007).
14. B. Li, N. Karpinsky, and S. Zhang, "Novel calibration method for structured light system with an out-of-focus projector," Appl. Opt. **53**, 3415–3426 (2014).